Int. J. Heat Mass Transfer. Vol. 33, No. 8, pp. 1619–1632, 1990
Printed in Great Britain

0017-9310/90 $3.00 + 0.00

Double-diffusive convection in a rectangle with opposing horizontal temperature and concentration gradients

JIN WOOK LEE and JAE MIN HYUN†

Department of Mechanical Engineering, Korea Advanced Institute of Science and Technology, P.O. Box 150, Chong Ryang, Seoul, Korea

(*Received* 13 *June* 1989)

Abstract—A numerical study is made of double-diffusive convection in a rectangular cavity with combined horizontal temperature and concentration gradients. The boundary conditions at the vertical side walls are imposed in such a way that the thermal and solutal buoyancy effects are counteracting, resulting in an opposing gradient flow configuration. Numerical solutions to the governing full time-dependent Navier–Stokes equations at large thermal (R_t) and solutal (R_s) Rayleigh numbers are acquired. The essential details of flow, temperature and concentration fields are described for a large Lewis number. The time evolutions of these fields are portrayed. Distinct flow regimes in the steady-state are identified as the buoyancy ratio R_ρ ($= R_s/R_t$) varies over a wide range. The structures of the thermal, solutal and velocity boundary layers near the side wall are examined. When R_ρ is moderate, the multi-layered flow structure in the interior is clearly depicted; the attendant S-shaped thermal field and the step-like concentration distribution are brought into focus. The existence of the layered flow structure in the core is strongly corroborative of the results of the prior experimental visualizations. Based on the numerical data, the steady-state mean Nusselt number $\overline{Nu}$ and Sherwood number $\overline{Sh}$ are tabulated for varying values of R_ρ. As R_ρ increases from a very small value, $\overline{Nu}$ decreases monotonically towards a value characteristic of conductive transfer; however, $\overline{Sh}$ reaches a minimum value when R_ρ takes a moderate value. This behavior is qualitatively consistent with the previous experimental findings.

1. INTRODUCTION

DOUBLE-DIFFUSIVE phenomena usually refer to a class of fluid motions which are subject to the simultaneous presence of two (or possibly more) diffusive components with different molecular diffusivities [1]. In the initial stages of development of this topic, much of the research was devoted to applications in the oceanic flow processes; the primary diffusing agents are heat and salt in this case, and the process has accordingly been termed thermohaline or thermosolutal convection. A growing body of literature has since been produced, elucidating salient features of many fluid systems, with particular reference given to the convective phenomena in the oceans. Among others, such classical flow behavior as the salt fountain or the oscillator has been well documented, and some of these illustrative flows have been demonstrated in simple laboratory experiments [1].

Expanding further on the subject of double-diffusion, mostly along the analytical and experimental lines of approach, a more elaborate and subtle nature of the flows of a confined fluid has been disclosed for a variety of flow geometries and boundary conditions. Some of the prominent laboratory studies include those of Turner [2], Huppert and Linden [3], and Incropera and Viskanta [4]. These investigations dealt with the flow structure in a fluid system in a container with a vertically stable density gradient when heating was applied at the bottom wall. One striking feature of these revelations was the presence of the layered flow structure. The precise details of the flow properties of the layer structure showed marked variations depending on the specific boundary conditions; however, the formation of layers and interfaces was predicted theoretically and was verified experimentally for some specific examples.

Another interesting flow configuration of a contained fluid can be found in a system with a vertically stable salinity gradient subject to horizontal heating (or cooling). The forming of the layered structure and the horizontal propagation of the convective cells are eminent features of this fluid system. This problem was originally conceived by Thorpe *et al.* [5], who made analytical predictions and experimental observations regarding the existence of the layered structures. Some discrepancies in the flow properties were noted, and subsequent efforts [6] were directed to clarify the details of the flow characteristics. Laboratory flow visualizations by Wirtz *et al.* [7] succinctly demonstrated the essence of the layer structure of the flow in an enclosure, in which a vertical concentration gradient and a horizontal temperature gradient were imposed on the container boundaries.

As in the foregoing statements, the bulk of the prior

† Author to whom all correspondence should be addressed.

NOMENCLATURE

Ar aspect ratio, H/L
C_h dimensional concentration at the high-concentration side wall
C_l dimensional concentration at the low-concentration side wall
C_0 dimensional reference concentration
ΔC concentration difference, $C_h - C_l$
D mass diffusivity
g gravity
H height of cavity
L width of cavity
Le Lewis number, κ/D
$\overline{Nu}$ local Nusselt number
$\overline{Nu}$ mean Nusselt number
P nondimensional pressure
p dimensional pressure
Pr Prandtl number, ν/κ
R_s solutal Rayleigh number, $g\beta_s\Delta C L^3/\kappa\nu$
R_t thermal Rayleigh number, $g\beta_t\Delta\theta L^3/\kappa\nu$
R_ρ buoyancy ratio, $\beta_s\Delta C/\beta_t\Delta\theta$
S nondimensional concentration
Sc Schmidt number, ν/D
$\overline{Sh}$ local Sherwood number
$\overline{Sh}$ mean Sherwood number
T nondimensional temperature
t dimensional time
U nondimensionalized horizontal velocity component
u dimensional horizontal velocity component
V nondimensionalized vertical velocity component
v dimensional vertical velocity component
X nondimensional horizontal coordinate
x dimensional horizontal coordinate
Y nondimensional vertical coordinate
y dimensional vertical coordinate.

Greek symbols
β_s coefficient of volumetric expansion with concentration
β_t coefficient of volumetric expansion with temperature
δ_s solutal boundary layer thickness
δ_t thermal boundary layer thickness
θ_h dimensional temperature at the high-temperature side wall
θ_l dimensional temperature at the low-temperature side wall
θ_0 dimensional reference temperature
$\Delta\theta$ temperature difference, $\theta_h - \theta_l$
κ thermal diffusivity
ν kinematic viscosity
ρ dimensional density
ρ^* nondimensional density
ρ_0 dimensional reference density
τ nondimensional time
τ_h nondimensional heat-up time scale
τ_s nondimensional 'e-folding time' for a purely solutal convection
ψ nondimensional stream function.

work was concerned with the flow configuration in which the concentration gradient was applied in the vertical direction. Obviously, this was consistent with the flow models of relevance to the oceanic fluid systems. However, recent industrial developments in modern technological innovations have increased the need for high quality material processing. The growth of crystals, chiefly used in electromechanical industries, is a prime example. The heat and mass transport phenomena in the fluid phase associated with material processing are critical to the quality and productivity of the crystals grown.

For the flow models of great value for engineering applications in material processing, the problem of double-diffusive convection in a confined space is a central issue. The diffusive properties are usually concentration of a substance (such as impurity or dopant) and heat. A clear understanding of the fluid transport phenomena that arise in this kind of convective flow bears an added significance as the material processing activities gain momentum by exploiting the reduced-gravity environment of space vehicles [8]. As pointed out by Ostrach [9], various modes of convection, exhibiting their particular characteristics, are possible depending on the flow configuration and the externally specified boundary conditions. Some of the prominent conditions are, among others, the strength and direction of the gradients of the diffusive properties imposed on the fluid system.

One outstanding flow configuration is the double-diffusive natural convection in a cavity with both the externally imposed temperature and concentration gradients normal to the gravity vector. This flow represents an idealization of many realistic fluid systems that are frequently utilized in growing high quality crystals. In spite of the apparent relevance to technological applications, as observed by Wang *et al.* [10], this flow model has remained largely untreated in the literature. Apart from the practical utility, this flow poses a problem of substantial interest in basic fluid dynamics. Ostrach [9] asserted that the qualitative flow characteristics are heavily influenced by the orientations of the gradients of the diffusive agents relative to the gravity vector. Wang *et al.* [10] and

Kamotani *et al.* [11] initiated preliminary experiments in a rectangular cavity of aspect ratio 0.55. They used an electrochemical system in a copper sulfate–acid solution to simulate the horizontal concentration gradient. The experiments revealed a three-layered flow structure in the core for a certain range of buoyancy ratio. These experimental endeavors were, however, highly restrictive in nature. The above experiments were limited to the early stages of convection, and they were unable to perform the experiments leading to the steady-state. Owing to the unavoidable thermal convection and electrolysis, the imposed horizontal concentration gradient could not be held constant. Recently, Lee *et al.* [12] and Lee and Hyun [13] devised improved experimental techniques by installing vertical membrane walls; exterior to these membranes, solutions of constant preset concentration and temperature were forced to circulate. In this manner, Lee *et al.* [12] and Lee and Hyun [13] achieved a closer experimental approximation to the steady-state gradients of both temperature and concentration imposed in the horizontal direction in the rectangular cavity. Lee *et al.* [12] and Lee and Hyun [13] observed the layered flow structure in the rectangular enclosures of aspect ratio 2.0 and 0.2. For the flows in a vertical slot, scaling analyses were performed by Bejan [14] under the restrictive assumptions that the inertia terms were neglected. His analyses were concerned mainly with the two extreme cases in which the buoyancy effect was dominated either by heat transfer or by mass transfer from the sides.

In brief, as documented above, the recent accomplishments on the experimental front of these complex flow phenomena have been remarkable. However, these experimental findings have not been critically assessed against other independent investigations. One powerful and highly versatile avenue of research will be comprehensive and explicit numerical studies. Obviously, the properly conducted numerical approaches will validate the essential elements of the experimental measurements; furthermore, the numerical solutions are capable of illuminating the wealth of details of the flow properties, which are not normally available by experimental techniques alone. The numerical endeavors will therefore be highly complementary to the experimental studies. The full-dress numerical simulations in the past encountered formidable difficulties due principally to the problem of the numerical solution techniques and the prohibitive computational costs. For realistic double-diffusive convections with large Lewis numbers, the solutal boundary layer is much thinner than the thermal boundary layer. Resolving this thin solutal layer requires excessively large computing resources, and this has been one main factor hampering the progress in numerical studies of the problem in hand. In the present paper, by taking advantage of the greatly expanded modern computing capabilities, we have carried out numerical calculations of the governing, full time-dependent Navier–Stokes equations. In an effort to isolate and elucidate the physics involved, double-diffusive convection in a rectangular cavity with both the temperature and concentration gradients applied in the horizontal direction is considered. The primary aim of the present study is to describe clearly the pertinent characteristics of flow, temperature and concentration fields in the cavity. We shall demonstrate the details of the layered flow structure and the profiles of the flow properties. The major impetus will be given to ascertaining the effect of the buoyancy ratio ($R_\rho = R_s/R_t$), R_s and R_t being the solutal and thermal Rayleigh numbers, on the flow structures.

In the present study, the thermal and solutal boundary conditions on the vertical side walls of the rectangular container are imposed such that both the temperature and concentration on one vertical side wall are higher than those on the other vertical side wall. This implies that the buoyant convections driven by the two horizontally parallel gradients are counteracting, which has been termed the opposing case [9]. The horizontal top and bottom walls are insulated and impermeable. The opposite configuration, in which the two imposed horizontal gradients of temperature and concentration are antiparallel, constitutes the cooperating case [9]; this problem will be dealt with in a subsequent companion paper [15].

Comprehensive and systematically organized numerical solutions have been acquired for high solutal and thermal Rayleigh numbers. The calculations have covered a wide range of the buoyancy ratio ($R_\rho = 0.5$–30). The time evolutions of the flow, thermal and solutal fields will be examined. These numerical results will be shown to be in broad qualitative consistency with the available experimental observations [11–13]. By analyzing the numerical data, the heat and mass transfer coefficients on the boundary wall have been computed. This information has not been readily provided by the prior experimental efforts [12]. The present numerical studies will depict the essentials of the evolving layered flow structure and the behavior of the boundary layers, and will delineate the complex interactions of the diffusive agents in determining the flow patterns inside the cavity.

2. MATHEMATICAL FORMULATIONS

Figure 1 displays a schematic of the flow configuration. The rectangular cavity is of width L and height H, and the Cartesian coordinates (x, y), with the corresponding velocity components (u, v), are indicated herein. Initially, the fluid is motionless, and the temperature and concentration are uniform throughout at θ_0 and C_0, respectively. At the initial instant $t = 0$, the temperature and concentration at the vertical side walls are abruptly altered, and they are maintained thereafter. The governing equations are the two-dimensional, time-dependent Navier–Stokes equations with the Boussinesq assumptions incorporated. These equations, expressed in properly non-

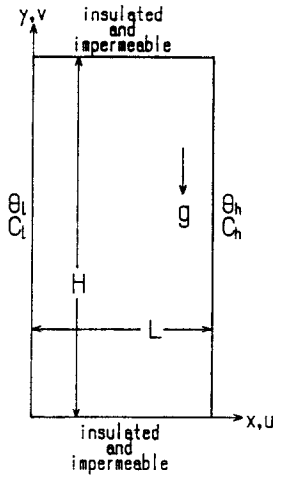

Fig. 1. Flow configuration and coordinate system.

dimensionalized form using standard notation, are well known [9]:

$$\frac{\partial U}{\partial X}+\frac{\partial V}{\partial Y}=0 \tag{1}$$

$$\frac{\partial U}{\partial \tau}+\frac{\partial}{\partial X}(UU)+\frac{\partial}{\partial Y}(VU)=-\frac{\partial P}{\partial X}+Pr\left(\frac{\partial^2 U}{\partial X^2}+\frac{\partial^2 U}{\partial Y^2}\right) \tag{2}$$

$$\frac{\partial V}{\partial \tau}+\frac{\partial}{\partial X}(UV)+\frac{\partial}{\partial Y}(VV)=-\frac{\partial P}{\partial Y}+Pr\left(\frac{\partial^2 V}{\partial X^2}+\frac{\partial^2 V}{\partial Y^2}\right)+Pr(R_t T-R_s S) \tag{3}$$

$$\frac{\partial T}{\partial \tau}+\frac{\partial}{\partial X}(UT)+\frac{\partial}{\partial Y}(VT)=\left(\frac{\partial^2 T}{\partial X^2}+\frac{\partial^2 T}{\partial Y^2}\right) \tag{4}$$

$$\frac{\partial S}{\partial \tau}+\frac{\partial}{\partial X}(US)+\frac{\partial}{\partial Y}(VS)=\frac{1}{Le}\left(\frac{\partial^2 S}{\partial X^2}+\frac{\partial^2 S}{\partial Y^2}\right). \tag{5}$$

In the above, the nondimensional quantities are defined as

$$U=[u/(\kappa/L)],\quad V=[v/(\kappa/L)],\quad X=x/L,$$
$$Y=y/L,\quad \tau=[t/(L^2/\kappa)],\quad P=p/(\rho\kappa^2/L^2),$$
$$T=(\theta-\theta_0)/(\theta_h-\theta_l),\quad S=(C-C_0)/(C_h-C_l),$$
$$Pr=\nu/\kappa,\quad Le=\kappa/D,\quad Ar=H/L,$$
$$R_t=g\beta_t\Delta\theta L^3/\kappa\nu,\quad R_s=g\beta_s\Delta C L^3/\kappa\nu,$$
$$R_\rho=(\beta_s\Delta C)/(\beta_t\Delta\theta)=R_s/R_t.$$

The dimensional temperature is denoted by θ, and the dimensional concentration of the heavier species by C. The physical properties are ν, kinematic viscosity; κ, thermal diffusivity; D, diffusivity of the concentration; β_t and β_s, the coefficients of volume expansion by thermal and concentration differences respectively. The maximum temperature and concentration differences across the cavity width are represented by $\Delta\theta=\theta_h-\theta_l$, and $\Delta C=C_h-C_l$. The principal nondimensional parameters are the Prandtl number Pr, the Lewis number Le, the thermal Rayleigh number R_t, the solutal Rayleigh number R_s and the aspect ratio of the container Ar. In the present study, the Prandtl number Pr and the Lewis number Le are set to be 7.0 and 100.0, respectively, to simulate the approximate values of salt water. The aspect ratio is set $Ar(=H/L)=2.0$ to allow explicit comparisons with the experiments of Lee *et al.* [12]. The solutal Rayleigh number R_s is set to be 6×10^7; in line with the basic objectives of the present study, the thermal Rayleigh number R_t, thus effectively the buoyancy ratio R_ρ, is varied to explore the various characteristic regimes.

The appropriate initial and boundary conditions are

$$U=V=T=S=0 \quad \text{at} \quad \tau=0; \tag{6}$$

$$U=V=0 \text{ on all solid boundaries}; \tag{7}$$

$$T=S=-0.5 \text{ on } X=0,\quad T=S=0.5 \text{ on } X=1; \tag{8}$$

$$\frac{\partial T}{\partial Y}=\frac{\partial S}{\partial Y}=0 \quad \text{on} \quad Y=0, Ar. \tag{9}$$

For definiteness, in the ensuing discussion, the left vertical wall ($X=0$) denotes the low-temperature and low-concentration boundary, and the right vertical wall ($X=1$) indicates the high-temperature and high-concentration boundary of the container; therefore, $C_0=(C_h+C_l)/2$, and $\theta_0=(\theta_h+\theta_l)/2$.

Numerical techniques to solve the above set of equations have been well established. After having tested rigorously several numerical algorithms, we have adopted a version of the EL2D program, based on the SIMPLER algorithm originally developed by Patankar [16]. The reader is referred to Patankar [16] for the specifics of the numerical methods. One of the main obstacles to the previous numerical attempts has been associated with the requirements of prohibitively large computing resources, although the numerical procedures themselves are fairly straightforward. In the present study, the entire computations were executed on a CRAY-2S super-computer. The mesh points employed were typically (51×75). A highly stretched grid net, in particular in the regions close to the vertical side walls, was needed to resolve the solutal boundary layer at large Lewis numbers.

3. RESULTS AND DISCUSSION

In order to gain a physical insight into the main features of the flow in the early phases, an illustrative stream pattern is displayed by plotting contours of

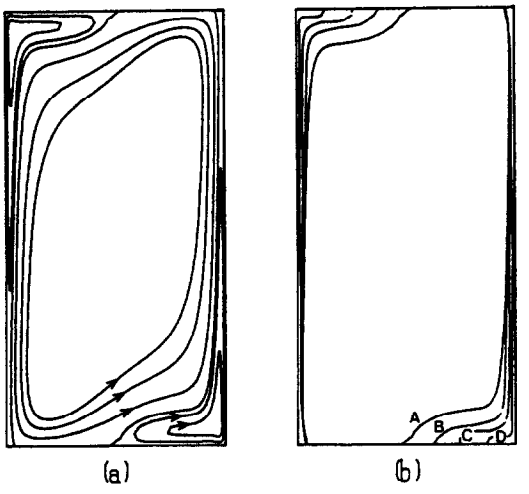

FIG. 2. (a) Illustrative stream pattern at a small time ($\tau = 0.004$). (b) Dividing streamlines at $\tau = 0.004$. Buoyancy ratios are $R_\rho = 20$ (A), 12.5 (B), 9 (C) and 6 (D).

the stream function ψ in Fig. 2(a). Here, the stream function ψ is defined such that $U = \partial\psi/\partial Y$, $V = -\partial\psi/\partial X$. The thermal diffusivity is much larger than the solutal diffusivity at large Lewis numbers; therefore, the thermal buoyancy is dominant in much of the region near the vertical boundaries. Only in very narrow strips adjacent to the vertical walls is the solutal buoyancy force substantial. Consequently, the heavier fluids in the narrow vicinities of the high-concentration vertical wall at $X = 1$ flow down toward the bottom horizontal wall. The downward flow within the extremely thin solutal boundary layer near $X = 1$ reaches the bottom horizontal wall at $Y = 0$, and advances along the horizontal wall toward the vertical wall at $X = 0$. This leftward horizontally moving flow is retarded by the thermally-induced flow which moves rightward near the bottom horizontal wall and upward near the hot vertical wall at $X = 1$. Therefore, in the right bottom corner, a clockwise closed circulation is formed by the above-described simultaneous action of solutally- and thermally-induced buoyancy effects. A similar, but antisymmetric, flow pattern is seen near the vertical wall at $X = 0$.

The extent of the horizontal advance of the corner closed circulation depends largely on the relative strength of the solutal buoyancy, i.e. R_ρ. Figure 2(b) demonstrates the location of the dividing streamline separating the corner circulation at a small time ($\tau = 0.004$) for varying buoyancy ratios. Obviously, as the buoyancy ratio increases, the horizontal layers that separate the corner circulations advance further toward the opposite vertical walls. This behavior was experimentally observed by Ostrach *et al.* [17] in a shallow cavity ($Ar = 0.13$).

The salient features of the flow at a large time close to the steady-state, when the buoyancy ratio is small, are illustrated in Fig. 3. The thermal field in the interior core shows a near-linear vertical stratification. Since the thermal effect is dominant in this case, i.e. a low R_ρ, the flow structure is akin to a single-diffusive purely thermal convection. The isohalines are highly concentrated in extremely thin regions near the vertical side walls. The strong thermal buoyancy obstructs the diffusion of concentration into the core; this causes the concentration in the core to maintain the original value of $S = 0.0$. In the bulk of the interior core, the counter-clockwise circulation, driven by the thermal buoyancy, is prevalent. In tiny localized regions near the top right and bottom left corners, the temperature gradients are relatively weak and the resulting weak clockwise circulations, induced by the solutal buoyancy, are visible.

The numerical results for an intermediate buoyancy ratio ($R_\rho = 12.5$) are depicted in Figs. 4–6. The thermal and solutal buoyancy effects are comparable in these situations. Figure 4 exemplifies the horizontal profiles of the temperature, concentration and vertical velocity in the core at mid-depth ($Y = Ar/2$) on the side of the low concentration wall ($X < 0.5$) at a large time ($\tau = 1.0$). The plots confirm that, at a large Lewis number ($Le = 100.0$), the solutal boundary layer thickness is much smaller than that of the thermal boundary layer. The flow is upward in the thin solutal boundary layer due to the low-concentration wall; outside of the solutal layer but within the thicker thermal layer, the flow is directed downward owing to the thermal buoyancy force. Wang *et al.* [10] suggested that, for a single-diffusive thermal or solutal convection, the ratio of the side wall thermal and solutal boundary layer thickness for $Pr > 1$ and $Sc > 1$ could be scaled as $\delta_t/\delta_s = (Le\, R_\rho)^{1/4}$. Inspection of the numerical results of Fig. 4 points to consistency with the above estimates of the layer thicknesses. Note that the present computations were for the case of a simultaneous application of the two buoyancy effects. This apparent consistency, therefore, implies that the coupling between mass diffusion and heat conduction within these boundary layers is relatively weak and, consequently, it is believed that the thicknesses of the two layers could be estimated quite independently.

Figure 5 displays the time evolution of thermal, solutal and flow fields. Also shown is the vertical profile of the horizontal velocity along the mid-width $X = 0.5$. At very early times (see Fig. 5(a) for $\tau = 0.004$), the thermal field is generally very similar to that of a pure thermal convection. Only in narrow strips adjacent to the vertical side walls is the flow driven by the solutal buoyancy discernible. As remarked earlier, the solutal diffusivity is much smaller than the thermal diffusivity; the isohalines are crowded only very near the vertical walls, and the bulk of the container interior is still at the uniform concentration $S = 0.0$. Figure 5(b) illustrates the results at a small time, $\tau = 0.05$. However, notice that this corresponds to a time instant which is much larger than the conventional heat-up time scale. For the parameter values of Fig. 5, the heat-up time scale, given by $\tau_h = 2^{-1/2} Ar^{1/4} R_T^{-1/4}$ [18], is $\tau_h = 0.0180$.

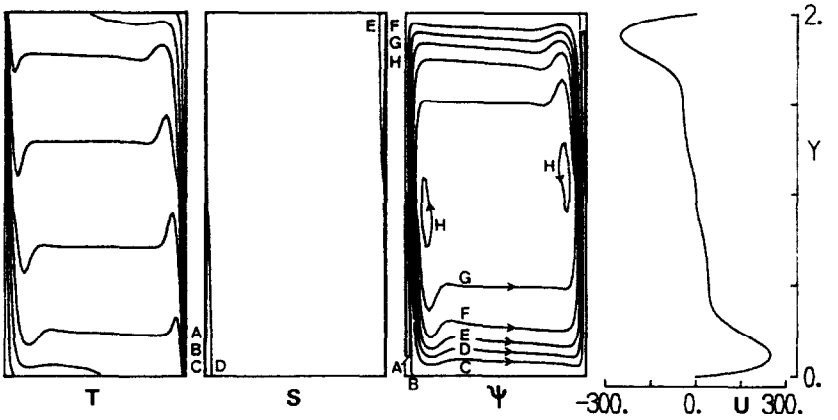

FIG. 3. Plots of isotherms, isohalines, stream functions and the vertical profile of horizontal velocity at mid-width. Conditions are $R_\rho = 3.0$ and $\tau = 1.0$. Values for isotherms are, from left to right, -0.389, -0.278, -0.167, -0.0556, 0.0556, 0.167, 0.278 and 0.389. Values for isohalines are: A, -0.389; B, -0.278; C, -0.167; D, -0.0556; E, 0.0556; F, 0.167; G, 0.278; H, 0.389. Values for ψ are: A, -1; B, 0; C, 13.5; D, 27; E, 40.5; F, 54; G, 67.5; H, 81.

Consequently, the thermal effect has penetrated well into the interior core, but the concentration in the greater part of the interior is still at the initial value of $S = 0.0$. Only in the top and bottom regions is the concentration stratified. The flows driven by the solutal buoyancy, which are opposite to the thermally-induced flows, predominate the boundary regions near the solid walls in the clockwise sense. In the core, the horizontal velocities are very weak, and the thermal field exhibits a linear vertical stratification. At intermediate times (see Fig. 5(c) at $\tau = 0.2$), the top and bottom regions, in which concentration is stratified, expand further toward the mid-depth. The counter-clockwise circulation in the core near the mid-depth, maintained by the thermal buoyancy, shrinks in size. The concentration is nearly uniform ($S = 0.0$) within this counter-clockwise circulation. In the regions between the edges of this counter-clockwise circulation cell and the top and bottom areas of clockwise flows, two more counter-clockwise cells begin to form. At large times (Fig. 5(d) at $\tau = 0.5$), this multi-layered flow structure becomes fully established. The thermal field illustrates a complicated pattern. It appears that the entire cavity breaks down into three mini-cavities corresponding to the three layer-structured counter-clockwise circulations in the core. As to the flow field, the small-sized secondary rolls, which are discernible within the primary counter-clockwise circulation at small and intermediate times, disappear at large times when the fully layered structure is developed. It is recalled that, for the case of a purely thermal convection at large thermal Rayleigh numbers, the secondary rolls exist near the vertical walls [19]. In the present numerical calculations, one may argue that the effective Rayleigh number for each mini-cavity is much smaller than the overall Rayleigh number for the entire system, pointing to the absence of the secondary rolls in the fully established state. Mention should be made of the experiments of Thorpe *et al.* [5] in which the solutal and thermal fields exhibited features similar to the above findings. It is noted that their experiments were performed with an imposed vertical concentration gradient and a horizontal temperature gradient. However, the physical interpretations are equally applicable to the layered structures in the interior core for both flow configurations. In order to examine the layered structure in further detail, the vertical profiles of T and S along the mid-width $X = 0.5$, as well as the local Nusselt number $Nu\,(=\partial T/\partial X|_{X=0})$ and the Sherwood number $Sh\,(=\partial S/\partial X|_{X=0})$, are plotted in Fig. 6. Three different time instants are represented in the figure to portray the evolutions. Evidently, when the layered structure has been established, the characteristic 'S'-shaped temperature profile and the step-like concentration distribution are readily recognized. Within each layer, the concentration is nearly uniform. This is attributable to vigorous convective mixings within the cell. Step-like changes in concentration take place at the interfaces of the two adjacent layers. Similar features were also observed in the experiments of Thorpe *et al.*

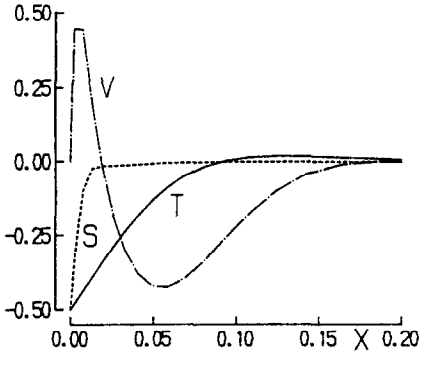

FIG. 4. Horizontal profiles of temperature (T), concentration (S) and vertical velocity ($V^* = V/500$) at mid-height ($Y = Ar/2$). Conditions are $R_\rho = 12.5$ and $\tau = 1.0$.

(see Figs. 12 and 13 of ref. [5]). Along the vertical side wall, the local Nu shows considerable dependence on the interior flow and thermal structures, but such dependence of Sh is relatively weak. This can be explained by noting that the influence of the global flow in the interior core on the structure within the solutal boundary layer is minor; very close to the vertical side walls, the solutally driven flow is the principal element in determining the features within the thin solutal boundary layer.

As the buoyancy ratio increases further, the effect of the solutal buoyancy outweighs the thermal effect. Figure 7 exemplifies the results with a large buoyancy ratio, $R_\rho = 30.0$. At small times (see Fig. 7(a) at $\tau = 0.05$), the region in which the solutal buoyancy is predominant occupies a comparatively larger portion of the cavity. Figures 7(a) and (b) show that, unlike the previous case of a moderate R_ρ, a two-layer structure is visible in the interior core, in which the thermal field is strongly stratified and the concentration is still at the initial, uniform value $S = 0.0$. Since the overall magnitude of the thermal buoyancy is small, the thermal fields near the vertical walls can be characterized as nearly conductive. Consequently, the boundary layer suction mechanism by the thermal buoyancy, which is the vital ingredient in a thermally convective process, is feeble. Furthermore, the clockwise circulation, driven by the strong solutal buoyancy, around the periphery of the vertical side walls is noticeable. The two-layer structure is discernible in the middle portions of the cavity, where the local thermal field contains areas of gravitationally unstable temperature distributions. As time elapses toward intermediate stages (see Fig. 7(b) at $\tau = 0.5$), the two layers are reduced in size and they tend to move closer to the mid-depth. At large times (see Fig. 7(c) at $\tau = 1.0$), the layered structure vanishes, and the flow field bears characteristics similar to a purely solutal convection. The concentration field is substantially linearly stratified in the vertical direction, and the thermal field in the bulk of the core resembles that of a conductive distribution. The velocities are appreciable only within very thin boundary layers adjacent to the solid walls, and the fluid in much of the interior is nearly stagnant.

Figure 8 reveals the explicit influence of the buoyancy ratio on the eminent features of the steady state ($\tau = 1.0$). This time instant, $\tau = 1.0$, corresponds to roughly three 'e-folding times' τ_s for a purely solutal convection, i.e. $\tau_s = 2^{-1/2} Ar^{1/4} Le^{3/4} R_s^{-1/4}$ [18]. Figure 8(a) demonstrates the results when R_ρ is substantial, i.e. $R_\rho = 20.0$ (note that this value of R_ρ is intermediate between the results of Figs. 5 and 7). The solutally driven flow is dominant in much of the entire cavity. Only in a narrow core region surrounding the mid-depth is the thermal buoyancy significant. Consequently, the overall flow pattern is clockwise, except in the small core where the thermally driven flow is in the counter-clockwise sense. Also, within this localized core region, the thermal layer is of convective boundary layer type, and the temperature is stratified while the concentration is at a uniform value ($S = 0.0$). Figure 8(b) for $R_\rho = 9.0$, and Fig. 8(c) for $R_\rho = 6.0$ clearly depict the changes in the flow characteristics as the buoyancy ratio decreases. As can be easily anticipated, the buoyancy ratios of Figs. 8(b) and (c) belong to the general category when the solutal and thermal effects are roughly comparable. An outstanding feature of the flow in these circumstances is the presence of the layered structure, which was succinctly ascertained earlier (see Fig. 5(d) for $R_\rho = 12.5$ at $\tau = 1.0$). However, a close inspection of these three sets of results points to measurable differences as well. As the buoyancy ratio decreases (or the relative thermal effect increases), it is noteworthy that the temperature gradients near the vertical walls become steeper; also, the top and bottom areas in which the concentration is stratified shrink in size. These observations are attributable to the more vigorous thermal convective activities. This has the implication that, as the buoyancy ratio decreases, the regions of the localized solutally-induced clockwise circulations near the top and bottom end walls become narrower. Figure 8(c) for $R_\rho = 6.0$ discloses that the solutally driven flows along the top and bottom walls have nearly disappeared. Scrutiny of the solutal fields of Figs. 8(b) and (c) also indicates that the intervals between the two isohalines at the layer interfaces become smaller as R_ρ decreases. This implies that the step-like variation of concentration becomes sharper and the thickness of the interface itself diminishes as R_ρ decreases. Accordingly, any further reduction in R_ρ brings forth the flow regime in which the thermal effect is predominant throughout the whole cavity, as was asserted earlier (see Fig. 3 for $R_\rho = 3.0$).

Based on the foregoing results, we may summarize the following four categories of flow regimes as R_ρ varies. These are: (1) the regime in which the thermal effect is fully dominant (e.g. Fig. 3), resembling a purely thermal convection; (2) the regime in which both the thermal and solutal effects are comparable (e.g. Figs. 5, 8(b) and (c))—the distinct layer structures are the characteristic features; (3) the regime in which the solutal effect is dominant, except within the mid-depth core region where the primary effect is thermally-induced (e.g. Fig. 8(a)); (4) the regime in which the solutal effect is fully dominant (e.g. Fig. 7), resembling a purely solutal convection. These categorizations are in full accord with the experimental characterizations of Lee *et al.* [12]. The experimental classifications of ref. [12] excluded regime (3) above. The close agreement exhibited between the present numerical results and the available experimental observations of ref. [12], both in the main flow characteristics and in the patterns of the thermal and solutal fields, is highly encouraging.

The explicit effect of the buoyancy ratio on the structures of the steady-state boundary layers is portrayed in Fig. 9. As R_ρ increases, the overall thermal

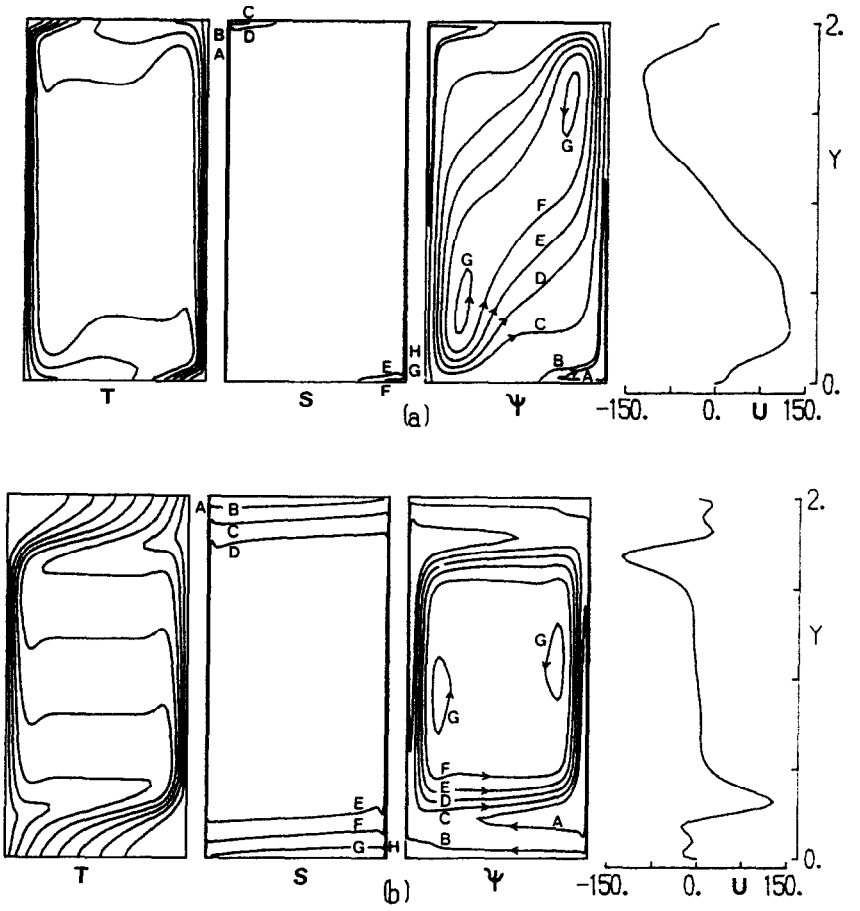

FIG. 5. Time evolving plots of isotherms, isohalines, stream functions and vertical profile of horizontal velocity at mid-width for $R_\rho = 12.5$. Times are $\tau = 0.004$ (a), 0.05 (b), 0.2 (c) and 0.5 (d). Values for isotherms and isohalines are the same as in Fig. 3. Values for ψ are: (a) A, −3; B, 0; C, 18; D, 36; E, 54; F, 72; G, 90; (b) A, −3; B, −1; C, 1; D, 6; E, 11; F, 16; G, 21; (c) A, −1.7; B, −0.9; C, 2; D, 6; E, 10; F, 14; (d) A, −2; B, −1; C, 3; D, 8; E, 13.

field changes its character from boundary layer type to conductive type, since the enhanced solutal stratification inhibits thermal convection in the cavity (see Fig. 7(c)). As expected, the concentration field becomes more strongly boundary layer type as R_ρ increases. The consequence in the flow structure, as R_ρ increases, appears in the augmentation of the vertical velocity within the thin solutal layer. Figure 9(c) demonstrates that the flow in much of the cavity, with the exception of the solutal layer, is determined primarily by the thermal effect, even though the solutal Rayleigh number R_s is larger than the thermal Rayleigh number R_t.

We shall examine in further detail the effect of R_ρ on the steady-state density structure. Figure 10 illustrates the vertical profiles at $\tau = 1.0$ of ρ^*

$$\rho^* = \frac{1}{\beta_s \Delta C}\left(\frac{\rho}{\rho_0} - 1\right) = -\frac{T}{R_\rho} + S$$

along the mid-width. When R_ρ is large (see the curve for $R_\rho = 30.0$), the density field is nearly linearly stratified in the vertical direction due to the dominant solutal buoyancy. For intermediate values of R_ρ, the aforementioned step-like density stratification, in association with the layered flow structure, is conspicuous. Further scrutiny of the numerical data of intermediate R_ρ, i.e. $R_\rho = 6.0$, 9.0 and 12.5, indicates that the height of the individual layer increases and the thickness of the layer interface decreases as R_ρ decreases. When R_ρ is very small (see the curve for $R_\rho = 3.0$), the density is weakly stratified, and the entire flow field is influenced principally by the thermal effect. It is noted, in passing, that localized patches in which the density field is almost constant or even slightly gravitationally unstable are visible near the top and bottom horizontal walls. As asserted earlier, when R_ρ is small, the counter-clockwise circulation, driven by the dominant thermal buoyancy, is strong enough to transport fluids of high (low) concentration from the right (left) side wall to the top (bottom) end wall; this mechanism sustains the above-described patches near the horizontal end walls.

We now turn to the question of the total heat and mass transfer rates across the cavity. These quantities

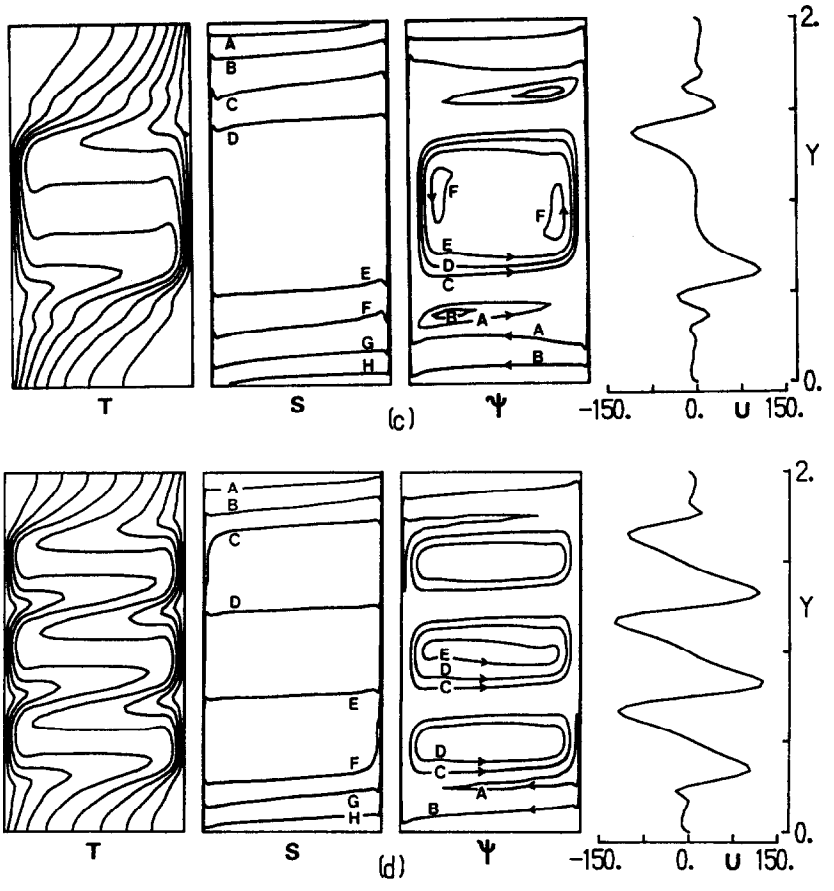

FIG. 5.—*Continued.*

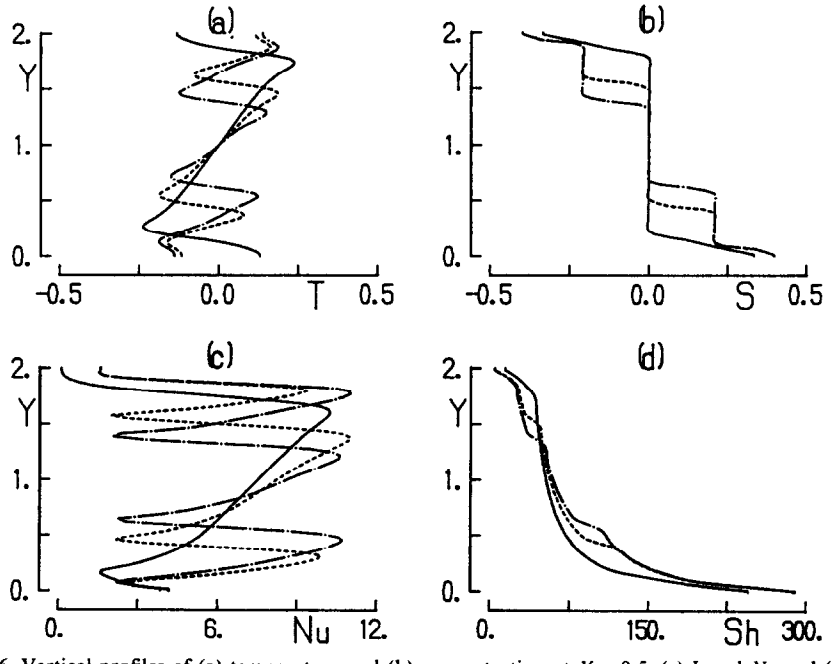

FIG. 6. Vertical profiles of (a) temperature and (b) concentration at $X = 0.5$. (c) Local Nu and (d) Sh at $X = 0$. The condition is $R_\rho = 12.5$. Times are: ——, $\tau = 0.05$; – – – –, $\tau = 0.2$; — · — · —, $\tau = 0.5$.

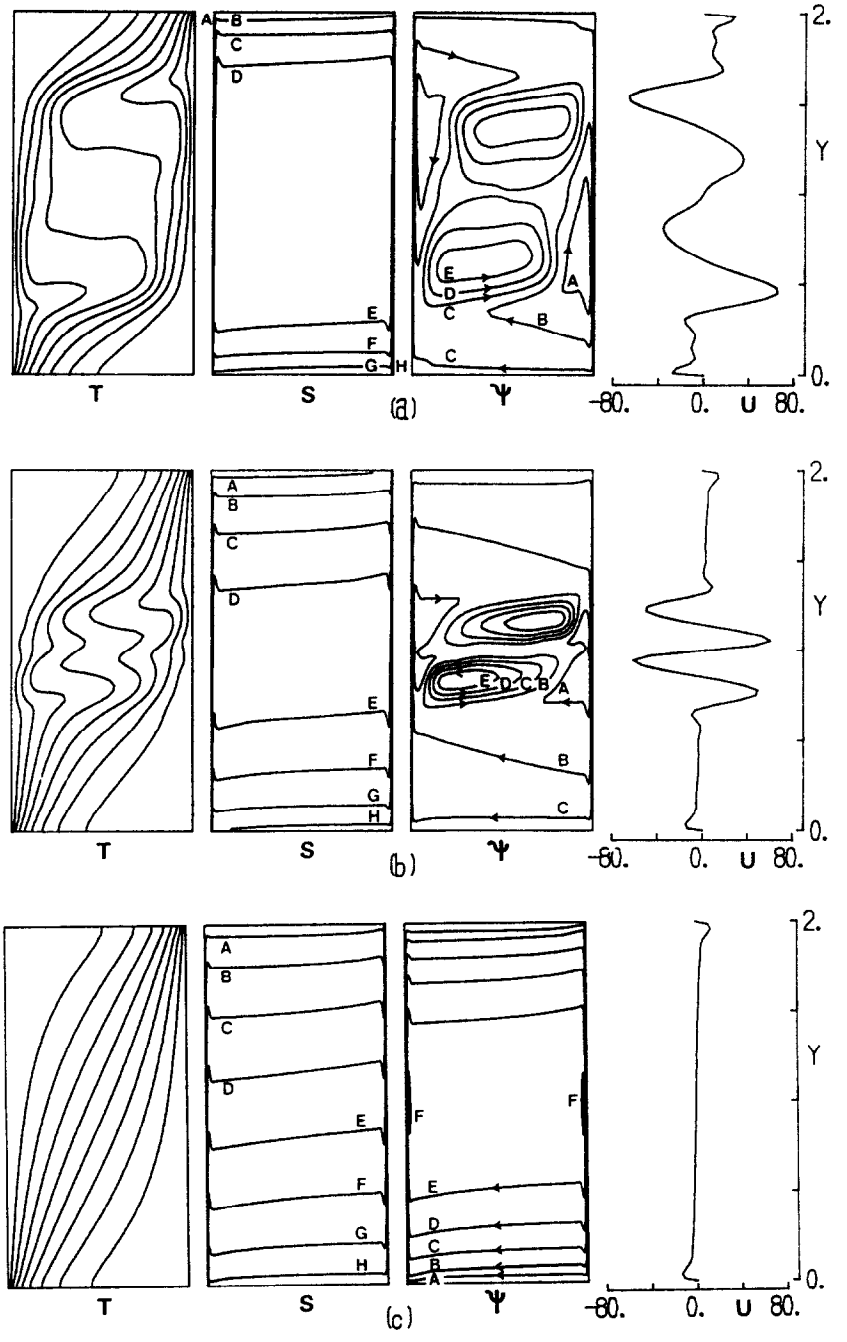

FIG. 7. Time evolving plots of isotherms, isohalines, stream functions and vertical profiles of horizontal velocity at mid-width. The condition is $R_\rho = 30.0$. Times are $\tau = 0.05$ (a), 0.2 (b) and 1.0 (c). Values for isotherms and isohalines are the same as in Fig. 3. Values for ψ are: (a) A, -7; B, -4; C, -1; D, 2; E, 5; (b) A, -4; B, -2.5; C, -1; D, 0.5; E, 2; (c) A, -0.5; B, -1; C, -1.5; D, -2; E, -2.5; F, -2.94.

are of central importance to technological applications. Table 1 lists the numerical results for the mean Nusselt $\overline{Nu}$ and Sherwood $\overline{Sh}$ numbers defined as

$$\overline{Nu} = \frac{1}{Ar}\int_0^{Ar} (\partial T/\partial X)_{X=0}\, dY$$

and

$$\overline{Sh} = \frac{1}{Ar}\int_0^{Ar} (\partial S/\partial X)_{X=0}\, dY.$$

These were computed by using the data at the instant $\tau = 1.0$, which corresponds to approximately $3\tau_s$. When R_ρ is either large or small, at this time instant, the flows are virtually in steady-state conditions. Even for intermediate values of R_ρ, it is recalled that the

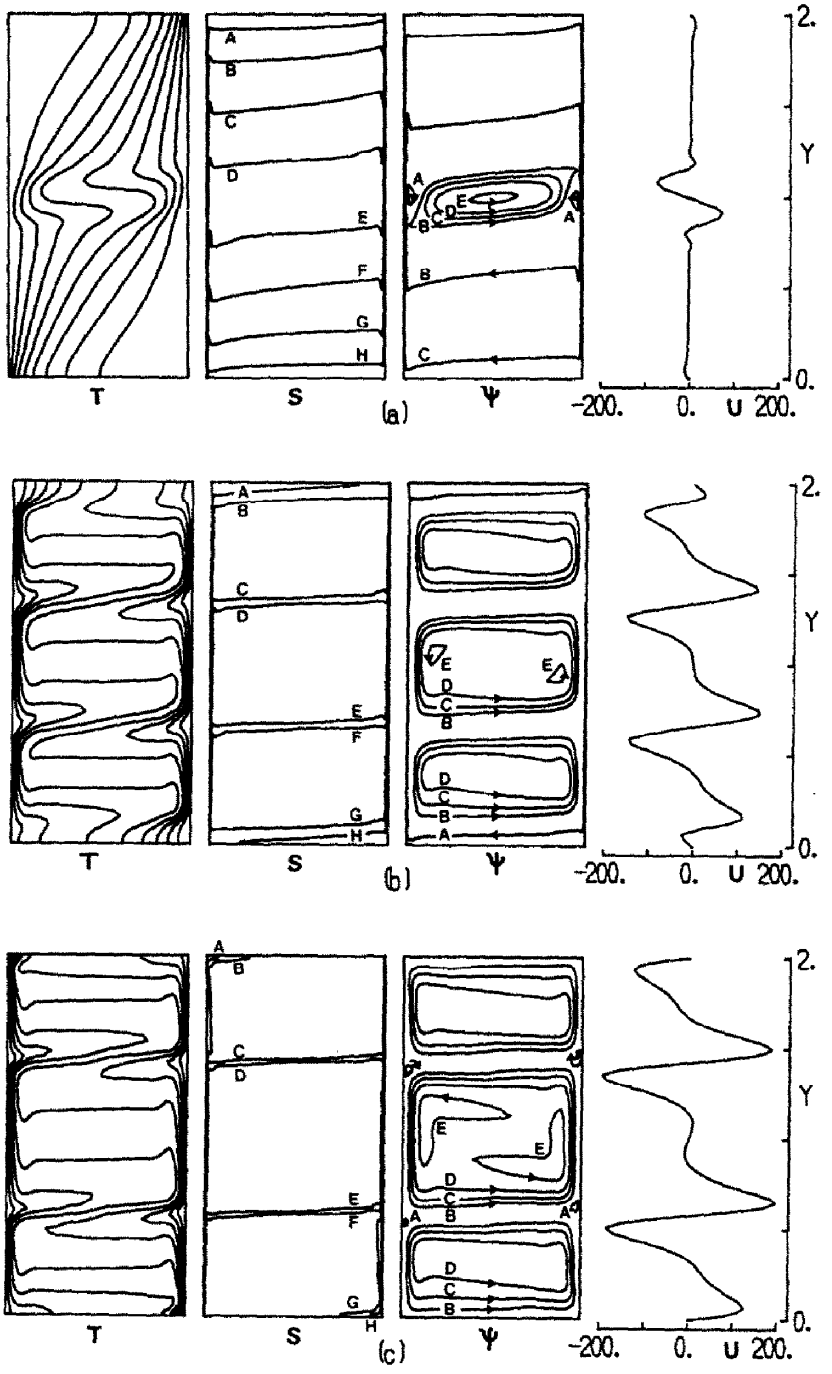

FIG. 8. Plots of isotherms, isohalines, stream functions and vertical profile of horizontal velocity at mid-width ($\tau = 1.0$). Buoyancy ratios are $R_\rho = 20$ (a), 9 (b) and 6 (c). Values for isotherms and isohalines are the same as in Fig. 3. Values for ψ are: (a) A, -4; B, -2.5; C, -1; D, 1; E, 4; (b) A, -0.8; B, 3.9; C, 8.6; D, 13.3; E, 18; (c) A, -3; B, 4; C, 11; D, 18; E, 25.

precise solutal boundary layer structure is substantially unaffected by the global interior flow after the e-folding time obtainable for pure solutal convection [11]. Also, the time variations in the interior flows are quite minor after about $3\tau_s$. Therefore, the numerical information for $\overline{Nu}$ and $\overline{Sh}$ in Table 1 represents the conditions at the steady-state or quasi-steady-state situations.

First, attention is focused on $\overline{Nu}$. Bejan [20], for the case of pure thermal convection, proposed a theoretically-derived expression for cavities of high aspect ratios ($Ar > 1$), $\overline{Nu} = 0.364(R_t/Ar)^{1/4}$ when $R_t^{1/7} Ar$

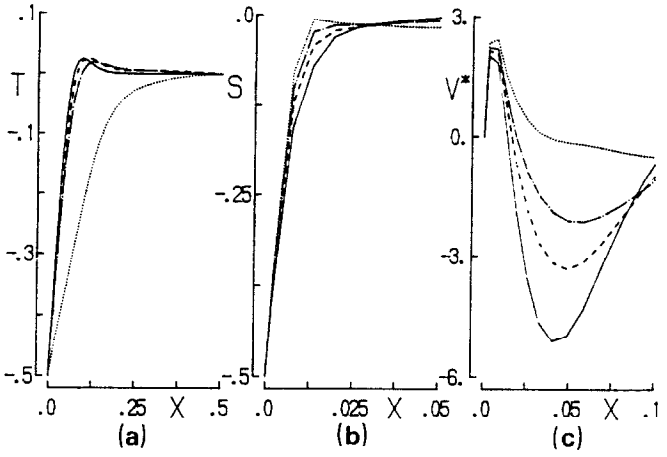

FIG. 9. Horizontal profiles of (a) temperature (T), (b) concentration (S), and (c) vertical velocity ($V^* = V/100$) near the low-temperature and low-concentration wall at $\tau = 1.0$. The values of R_ρ are: ——, $R_\rho = 6$; – – – –, $R_\rho = 9$; —·—·—, $R_\rho = 12.5$; ·····, $R_\rho = 20$.

tends to infinity. Although the present calculations are for large, but finite, values of $R_t^{1/7}Ar$, $\overline{Nu}$ computed for pure thermal convection in this study was found to be closely consistent with the prediction of ref. [20]. It should be noted that the value for PTC Nusselt number in Table 1 was obtained for the same R_t as the one assumed in each case of different R_ρ. When R_ρ is small, Table 1 indicates that $\overline{Nu}$ for a double-diffusive convection is slightly lower than that for the corresponding single-diffusive pure thermal convection. However, the discrepancies in the values of $\overline{Nu}$, which stem from the influence of the retarding solutal buoyancy effect, are insignificant. This can be explained as, for small values of R_ρ, the dominant role is played by thermal convection in the bulk of the cavity. On the contrary, when R_ρ is large, the influence of the counteracting solutal buoyancy is overwhelming. At extremely large values of R_ρ, the trend is that $\overline{Nu}$ approaches a value close to unity, suggesting that the thermal field is akin to that of a conduction-controlled case. This is the expected consequence of an inhibited thermal convection in the cavity due to a strong concentration stratification.

The behavior of the mass transfer is now delineated. As R_ρ increases towards moderate and large values, Table 1 shows that $\overline{Sh}$ tends to the limiting value appropriate for a purely solutal convection. It is noticeable that the increases in $\overline{Sh}$ are quite mild as R_ρ exceeds around 3.0, and the trend is more conspicuous when R_ρ takes larger values, say over 20.0. This can be explained by noting that, when R_ρ is large, the solutal boundary layer flow is the prime element in shaping up the overal flow pattern. The above observation is qualitatively consistent with the experimental findings of Kamotani *et al.* [11]. When R_ρ is sufficiently small, however, Table 1 shows that $\overline{Sh}$ increases rapidly as R_ρ decreases. This noteworthy behavior of $\overline{Sh}$ suggests that the mass transfer near the vertical wall is principally determined by the overriding thermal convection rather than by solutal con-

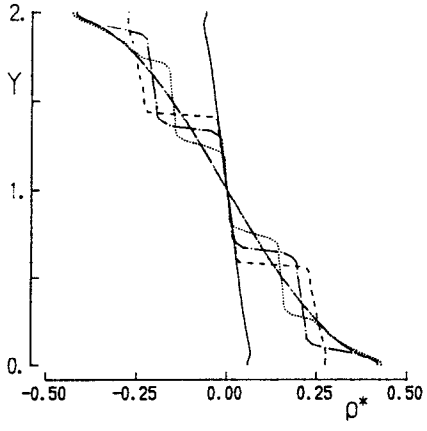

FIG. 10. Nondimensional density ρ^* at $X = 0.5$ at $\tau = 1.0$. The values of R_ρ are: ——, $R_\rho = 3$; – – – –, $R_\rho = 6$; —·—·—, $R_\rho = 9$; ·····, $R_\rho = 12.5$; —··—··—, $R_\rho = 30$.

Table 1. Mean Sherwood $\overline{Sh}$ and Nusselt $\overline{Nu}$ numbers at a large time ($\tau = 1.0$)

R_ρ	$\overline{Sh}$	$\overline{Nu}$ DDC	PTC
0.5	133.09	28.79	29.10
1.0	104.94	23.47	24.26
3.0	68.996	14.43	18.22
6.0	70.449	9.510	15.21
9.0	78.180	6.937	13.69
12.5	81.778	4.951	12.57
20.0	83.450	1.965	11.11
30.0	84.125	1.713	9.994
PSC	85.992		

For the tabulation of $\overline{Nu}$, DDC denotes the case of double-diffusive convection and PTC denotes the case of pure thermal convection. For the value of R_ρ, PSC indicates the case of pure solutal convection.

vection; at a very small R_ρ, the thermal buoyancy dominates the entire flow field, including the solutal boundary layer regions.

The above analyses of the behavior of $\overline{Sh}$, as seen in Table 1, point to the existence of a minimum $\overline{Sh}$ at a certain R_ρ. In the present numerical computations for $Le = 100.0$, this minimum of $\overline{Sh}$ occurs around $R_\rho \approx 3.0$. The presence of a minimum $\overline{Sh}$ was also pointed out by Kamotani *et al.* [11], and the results of the present numerical study are in broad qualitative consistency with their findings. Further examination of the present data and the experimental results of ref. [11] reveal some quantitative differences. At this juncture, two points can be raised for possible sources of the quantitative discrepancies. One is obviously due to the reduced side wall effect amenable for cavities of low aspect ratios ($Ar = 0.13$, 0.55) in the experiments of ref. [11]. Another might originate from the insufficient resolution in the present numerical results of the details within the extremely thin solutal layers. Use of a finer grid mesh could conceivably improve the numerical resolutions, which will provide far more accurate numerical flow data. These changes are reserved for future studies.

4. CONCLUSIONS

An extensive set of numerical results has been secured and examined to elucidate the flow details of time-dependent double-diffusive convection in a rectangular cavity of aspect ratio 2.0. The flows are driven by the horizontally imposed opposing temperature and concentration gradients.

In the early phases, the thermal buoyancy is dominant in much of the cavity due to the large difference between diffusivities of heat and solute, i.e. at large Lewis numbers.

The large-time behavior of the flows is strongly dependent on the buoyancy ratio, R_ρ. When R_ρ is very small or very large, the overall characteristics are similar to those of a single-diffusive thermal or solutal convection, respectively. However, when R_ρ is within a certain range of moderate values, a multi-layered flow structure is established in the interior core. The formation of the layered flow structure is a time-dependent process, and the substantial accomplishments of the flow processes are achieved over several e-folding time scales tenable for a purely solutal convection. With the layered flow structure, the characteristic S-shaped temperature field is discernible, and the step-like concentration distribution is conspicuous. The character of the individual layer is akin to a purely thermal convection in a mini-cavity of low aspect ratio. The interface of the layers is characterized by a stable but rapidly varying density distribution. These global flow patterns are in close agreement with the experimental visualization studies of Lee *et al.* [12].

Based on the numerical data, the steady-state mean Nusselt number $\overline{Nu}$ and Sherwood number $\overline{Sh}$ are acquired. As R_ρ increases from a very small value, $\overline{Nu}$ decreases monotonically, and at a large value of R_ρ, $\overline{Nu}$ is reduced towards a value appropriate for thermal conductive processes. However, $\overline{Sh}$ takes a minimum value when R_ρ is moderate, i.e. $R_\rho \approx 3.0$ in the present study. This qualitative behavior of heat and mass transfer rates is in accord with the experimental findings of Kamotani *et al.* [11].

Acknowledgements—The authors are grateful to the referee who provided detailed and constructive comments. This work was supported in part by a research grant from the Korea Science and Engineering Foundation (KOSEF).

REFERENCES

1. J. S. Turner, Double diffusive phenomena, *Ann. Rev. Fluid Mech.* **6**, 37–56 (1974).
2. J. S. Turner, The behavior of a stable salinity gradient heated from below, *J. Fluid Mech.* **33**, 183–200 (1968).
3. H. E. Huppert and P. F. Linden, On heating a stable salinity gradient from below, *J. Fluid Mech.* **95**, 431–464 (1979).
4. F. P. Incropera and R. Viskanta, Optical studies of mixed layer development in a double diffusive, thermohaline convection, *Proc. 7th Int. Heat Transfer Conf.*, Vol. 2, pp. 419–424 (1982).
5. S. A. Thorpe, P. K. Hutt and R. Soulsby, The effect of horizontal gradients on thermohaline convection, *J. Fluid Mech.* **38**, 375–400 (1969).
6. S. Thangam, A. Zebib and C. F. Chen, Double diffusive convection in an inclined fluid layer, *J. Fluid Mech.* **116**, 363–378 (1982).
7. R. A. Wirtz, D. G. Briggs and C. F. Chen, Physical and numerical experiments on layered convection in a density stratified fluid, *Geophys. Fluid Dyn.* **3**, 265–288 (1972).
8. S. Ostrach, Low-gravity fluid flows, *Ann. Rev. Fluid Mech.* **14**, 313–345 (1982).
9. S. Ostrach, Natural convection with combined driving forces, *PhysicoChem. Hydrodyn.* **1**, 233–247 (1980).
10. L. W. Wang, Y. Kamotani and S. Ostrach, Experimental study of natural convection in a shallow horizontal cavity with different end temperatures and concentrations, Report FTAS/TR-82-164, Case Western Reserve University (1983).
11. Y. Kamotani, L. W. Wang, S. Ostrach and D. Jiang, Experimental study of natural convection in shallow enclosures with horizontal temperature and concentration gradients, *Int. J. Heat Mass Transfer* **28**, 165–173 (1985).
12. J. Lee, M. T. Hyun and K. W. Kim, Natural convection in confined fluids with combined horizontal temperature and concentration gradients, *Int. J. Heat Mass Transfer* **31**, 1969–1977 (1988).
13. J. Lee and M. T. Hyun, Experiments on thermosolutal convection in a shallow rectangular enclosure, *Exp. Thermal Fluid Sci.* **1**, 259–265 (1988).
14. A. Bejan, Mass and heat transfer by natural convection in a vertical cavity, *Int. J. Heat Fluid Flow* **6**, 149–159 (1985).
15. J. M. Hyun and J. W. Lee, Double-diffusive convection in a rectangle with cooperating horizontal gradients of temperature and concentration, *Int. J. Heat Mass Transfer* **33**, 1605–1617 (1990).
16. S. V. Patankar, *Numerical Heat Transfer and Fluid Flow*. McGraw-Hill, New York (1980).
17. S. Ostrach, D. Jiang and Y. Kamotani, Thermosolutal convection in shallow enclosures, *Proc. ASME–JSME Thermal Engng Joint Conf.*, Vol. 2, pp. 159–168 (1987).

18. M. C. Jischke and R. T. Doty, Linearized buoyant motion in a closed container, *J. Fluid Mech.* **71**, 729–754 (1975).
19. J. M. Hyun and J. W. Lee, Transient natural convection in a square cavity of a fluid with temperature-dependent viscosity, *Int. J. Heat Fluid Flow* **9**, 278–285 (1988).
20. A. Bejan, A note on Gill's solution for free convection in a vertical enclosure, *J. Fluid Mech* **90**, 561–568 (1979).

CONVECTION DOUBLEMENT DIFFUSIVE DANS UN RECTANGLE AVEC DES GRADIENTS HORIZONTAUX OPPOSES DE TEMPERATURE ET DE CONCENTRATION

Résumé—On présente une étude numérique de la convection doublement diffusive dans une cavité rectangulaire avec gradients horizontaux combinés de température et de concentration. Les conditions aux limites sont imposées sur les faces verticales opposées de façon que les effets de flottement thermique et solutal se contrarient. On obtient des solutions numériques des équations de Navier–Stokes pour des grands nombres de Rayleigh thermique (R_t) et solutal (R_s) pour les champs de température et de concentration décrits à de grands nombres de Lewis. On décrit les évolutions dans le temps. Des régimes distincts en régime permanent sont identifiés quand le rapport de flottement R_ρ ($=R_t/R_s$) varie largement. On examine les structures des couches limites thermiques, solutales et dynamiques près des parois. On obtient la structure multicouche de l'écoulement quand R_ρ est modéré; le champ thermique en S et la distribution de concentration en escalier sont examinés. Les nombres de Nusselt $\overline{Nu}$ et de Sherwood $\overline{Sh}$ moyen sont tabulés pour des valeurs variables de R_ρ. Lorsque R_ρ augmente depuis une faible valeur, $\overline{Nu}$ décroît de façon monotone jusqu'à une valeur caractéristique de la conduction; néanmoins $\overline{Sh}$ atteint une valeur minimale quand R_ρ prend une valeur modérée. Ceci est qualitativement en accord avec des résultats expérimentaux antérieurs.

GEGENGERICHTETE DOPPELT-DIFFUSIVE KONVEKTION IN EINEM RECHTECKIGEN HOHLRAUM MIT HORIZONTALEN GRADIENTEN

Zusammenfassung—Die doppelt-diffusive Konvektion in einem rechteckigen Hohlraum mit waagerechten Temperatur- und Konzentrationsgradienten wird numerisch untersucht. Die Randbedingungen an den senkrechten Seitenwänden sind derartig, daß die thermischen und die konzentrationsbedingten Auftriebseffekte einander entgegenwirken. Die vollständigen zeitabhängigen Navier–Stokes-Gleichungen werden für große thermische (R_t) und Konzentrations- (R_s) Rayleigh-Zahlen berechnet. Das Strömungs-, Temperatur- und Konzentrations-Feld wird für eine große Lewis-Zahl ermittelt. Die zeitliche Entwicklung dieser Felder wird dargestellt. Es ergeben sich unterschiedliche stationäre Strömungsgebiete, abhängig vom Auftriebsverhältnis $R_\rho = R_s/R_t$. Die Struktur der Grenzschichten für Temperatur, Konzentration und Geschwindigkeit an der Seitenwand wird untersucht. Für mittlere Werte von R_ρ ergibt sich eine mehrschichtige Strömungsstruktur im Inneren; besonders betrachtet wird das S-förmige Temperaturfeld und die stufenförmige Konzentrationsverteilung. Die Existenz dieser geschichteten Strömung im Kern wird durch frühere experimentelle Versuche mit Sichtbarmachung der Strömung bestätigt. Aufgrund der numerischen Daten werden stationäre mittlere Nusselt-Zahlen ($\overline{Nu}$) und Sherwood-Zahlen ($\overline{Sh}$) für unterschiedliche Werte von R_ρ berechnet. Für kleine, zunehmende Werte von R_ρ nimmt die Nusselt-Zahl monoton bis auf einem Wert ab, der charakteristisch ist für Wärmeleitung; im Gegensatz dazu erreicht die Sherwood-Zahl für einen mittleren Wert von R_ρ ein Minimum. Dieses Verhalten stimmt qualitativ mit früheren experimentellen Beobachtungen überein.

КОНВЕКТИВНЫЙ ТЕПЛО- И МАССООБМЕН В ПРЯМОУГОЛЬНОЙ ПОЛОСТИ ПРИ ПРОТИВОДЕЙСТВУЮЩИХ ГОРИЗОНТАЛЬНЫХ ГРАДИЕНТАХ ТЕМПЕРАТУРЫ И КОНЦЕНТРАЦИИ

Аннотация—Численно исследуется конвективный тепло- и массообмен в прямоугольной полости с совместными горизонтальными градиентами температуры и концентрации. Граничные условия на боковых стенках таковы, что эффекты тепловых и массовых подъемных сил являются противоположными, что обусловливает характер течения с противодействующими градиентами. Получены численные решения полных нестационарных уравнений Навье–Стокса при больших значениях тепловых (R_t) и концентрационных (R_s) чисел Рэлея. Описаны характерные особенности полей течения, температур и концентраций для больших значений числа Льюиса. Проиллюстрирована эволюция этих полей во времени. При варьировании отношения подъемных сил $R_\rho(=R_s/R_t)$ в широком диапазоне значений обнаружено несколько различных стационарных режимов течения. Рассмотрены структуры теплового, массового и динамического пограничных слоев у боковой стенки. При умеренном значении числа R_ρ установлена четко выраженная многослойная структура течения во внутренней области; выявлены сопутствующие S-образное тепловое поле и ступенчатое распределение концентраций. Слоистая структура течения в ядре подтверждает результаты предыдущих экспериментальных наблюдений. На основе численных данных табулируются установившиеся средние значения чисел Нуссельта $\overline{Nu}$ и Шервуда $\overline{Sh}$ для различных значений числа R_ρ. При росте R_ρ от очень малого значения число $\overline{Nu}$ монотонно снижается до величины, характерной для кондуктивного теплопереноса, в то время как число $\overline{Sh}$ достигает минимума при умеренных значениях R_ρ. Такое поведение качественно согласуется с имеющимися экспериментальными данными.